Application of Cascode GaN HEMT in LLC Soft Switching Converter

Kaiyuan Qin[1], En Fang[1,2(✉)], and Yuan-ming Zhang[3]

[1] School of Electrical and Control Engineering, Xuzhou University of Technology, Xuzhou 221018, Jiangsu, China
fangen@cumt.edu.cn

[2] Jiangsu Key Construction Laboratory of Large Engineering Equipment Testing and Control Technology, Xuzhou 221018, Jiangsu, China

[3] State Grid Suqian Power Supply Company, Suqian 223800, Jiangsu, China

Abstract. After decades of development, the performance of Si-based power switching devices is approaching its material limits. The power electronic converter is limited to further growth in the direction of high frequency, high efficiency, and high power density. As an outstanding representative of the third generation of wide bandgap semiconductor devices, the cascode GaN HEMT utilizes a cascode structure to achieve the normally-off nature of GaN devices, with unmatched steady-state and dynamic performance of Si-based devices. In order to promote its replacement of Si devices and give full play to the performance advantages, the cascode GaN HEMT is applied to the soft-switching topology of the LLC resonant converter in this paper. The relationship between the output capacitance and the dead-time of the switching device is analyzed. The effects with root mean square values of the first and second side currents are also considered. Taking advantage of the small output capacitance of the cascode GaN HEMT, the circulating current of the converter is reduced, which leads to further reduction of the conduction and transformer loss. Thus, the efficiency of the converter is improved. An LLC converter with 97% maximum efficiency and 96.2% total load efficiency was built to prove the correctness and effectiveness of the analysis.

Keywords: Cascode GaN device · Hard switch · Soft switch · Application research

1 Introduction

High frequency, high efficiency, and high power density are the inevitable trend of the development of power electronic converters. High frequency is an effective way to reduce the volume of passive components and improve the converter's power density. However, with the increase of switching frequency, the switching loss and driving loss of the converter rise rapidly, which leads to the converter's efficiency reduction. With the development of power electronics in recent years, a few high-performance Si MOSFETs can reach a switching frequency of more than 1 MHz. But the switching speed

D. Jiang and H. Song (Eds.): SIMUtools 2021, LNICST 424, pp. 178–193, 2022.
https://doi.org/10.1007/978-3-030-97124-3_16

is still limited due to the significant parasitic parameters determined by their materials and packages, resulting in high switching and driving losses. So the devices can not be applied on a large scale. Therefore, in recent years, the development of power electronic converters mainly improves the power density and efficiency of the converter by researching the converter topologies and the performance of magnetic components.

Due to the material advantages of GaN devices and the reduction of parasitic parameters, the switching speed of GaN devices is much faster than that of Si MOSFETs. So it is possible to increase the switching frequency of the converters with GaN devices. The research on the static and dynamic characteristics and application of GaN devices is of great significance to improve the power density and efficiency of the converter.

The static and dynamic characteristics of the cascode GaN devices are different from those of traditional Si MOSFETs because of the unique structure and material aspects of the composite of Si MOSFET and GaN HEMT. Moreover, the change rate of voltage and current in the switching process of GaN devices is very high, and the influence of parasitic parameters at a low switching operation speed of GaN devices can not be ignored. The resulting voltage and current spikes and oscillations bring about the reliability reduction of the switching process, the switching loss increase, and the switching frequency limit of GaN devices. The advantages of GaN devices can not be fully utilized. Therefore, the parasitic parameters in the application of GaN devices are studied for optimization to reduce the switching loss and control the voltage and current spikes. The switching oscillation is critical to the application of GaN devices and also the inevitable choice to improve the power density, efficiency, and stability of GaN-based converters. At the same time, in soft-switching topology, it is an effective way to improve the efficiency of the soft-switching converter by using the smaller parasitic parameters of GaN devices to improve the conditions of soft switching and further reduce the converter loss.

In 2016, the industry market of gallium nitride power devices was about $12 million. In 2018, it accounted for 0.67% of the world semiconductor power market. The demand for gallium nitride power devices is expected to increase with explosive growth from 2018 to 2022, and the value will reach $450 million by 2022.

As the essential component of modern industry, China also attaches importance to the development of wide bandgap power devices. In the China-made 2025 plan, five major projects are proposed. In this plan, about the industrial foundation project, it is put forward that by 2020, 40% of the essential core parts and critical basic materials will be independently supported, including aerospace equipment, communication equipment, power generation, transmission equipment, rail transportation equipment and other equipment. The advanced manufacturing process of essential core components (components) and critical basic materials urgently needed by household appliances and other industries has been popularized and applied. By 2025, 70% of essential core parts and critical basic materials will be guaranteed independently. Therefore, accelerating the research and application of GaN power devices is also the need of the times and the nation, which is of great significance to enhance China's comprehensive competitiveness and support the world power status.

The factors that limit the frequency rise and stability of the cascode GaN HEMT in high-speed hard-switching applications are studied in this paper. And the devices are applied to a hard-switching buck converter. Under the given optimization measures, the

advantages of high-frequency and high-speed are brought into play, and the stability of the converter is guaranteed. Switching loss becomes the main part of system loss.

ZVS (zero voltage switch) is realized in LLC resonant soft-switching converter on the primary side and ZCS (zero current switch) on the secondary side. High energy conversion efficiency is achieved. In recent years, it has been widely used in switching power supply, LED-drive power supply, intermediate bus converter, power electronic transformer, and other occasions. In this chapter, the cascode GaN HEMT is applied to LLC resonant converter with a soft-switching topology. Using the characteristics of GaN device with small output junction capacitance, the converter's cycle current and dead time are reduced. The loss of the converter decreases and the efficiency of the converter is improved.

2 LLC Resonant Converter Principle

2.1 Circuit Topology

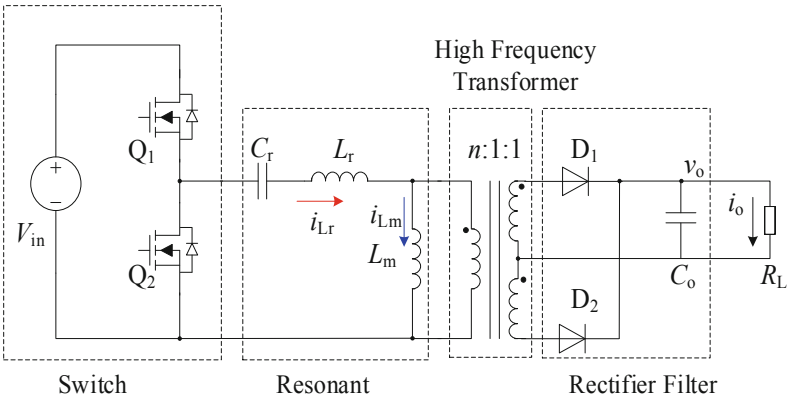

Fig. 1. Half-bridge LLC resonant converter topology.

Figure 1 shows the topology of the half-bridge LLC resonant converter, which mainly includes four parts. The switching network generates the square waves. The resonant network consists of resonant capacitor C_r, resonant inductor L_R, and excitation inductor L_m. The rectifier and filter network is composed of a high-frequency transformer with a middle tap, rectifier diode, and filter capacitor. The switching network consisting of main switches Q_1 and Q_2 generates a square wave voltage with a 50% duty cycle and adjustable frequency through complementary conduction. The dead time is inserted between the complementary conduction of Q_1 and Q_2 to prevent the bridge arm from passing through. Thus, ZVS on the primary side is realized. The impedance of the resonant network changes with the change of switching frequency, and the output voltage is adjusted with the switching frequency. The rectifier diodes D_1 and D_2 are full-wave rectified, and the output voltage is filtered by filter capacitor C_o.

2.2 Working Principle

The resonant network composed of resonant capacitor C_r, resonant inductor L_r and excitation inductor L_m has two resonant frequencies. The resonant frequency f_s of resonant capacitor C_r and resonant inductor L_r can be obtained by Eq. (1).

$$f_s = \frac{1}{2\pi\sqrt{L_r C_r}} \tag{1}$$

Resonant frequency f_m of resonant capacitor C_r and resonant inductor L_r can be driven from Eq. (2).

$$f_m = \frac{1}{2\pi\sqrt{(L_r + L_m)C_r}} \tag{2}$$

When the converter switching frequency f works in different load ranges, the system operates in three states. Figure 2 shows the waveforms of the converter working in different switching frequency ranges. LLC resonant converter can realize ZVS on the primary side in the entire load range and ZCS on the secondary side when $f_m < f < f_s$. The resonant network voltage is zero when the converter works at f = fs, and the efficiency reaches the maximum. Taking the converter working in $f_m < f < f_s$ state as an example, the working process of the converter is divided into six stages. The operational circuit diagrams of different phases are shown in Fig. 3, and working principles are analyzed in detail.

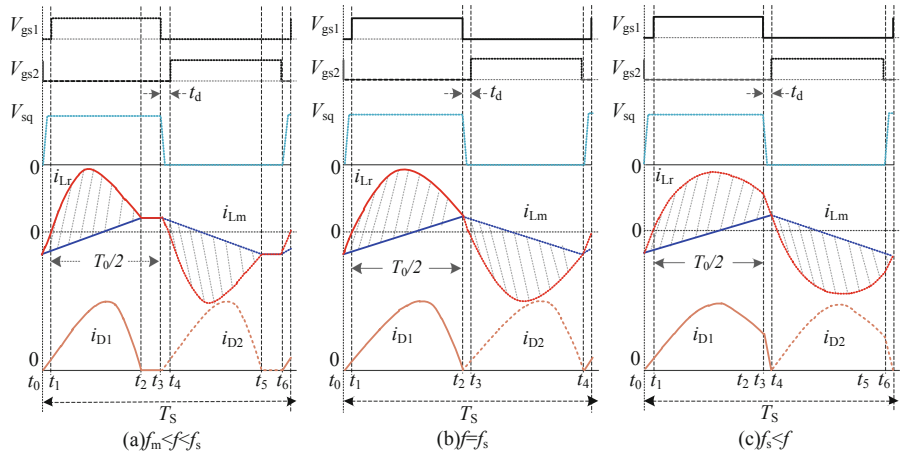

Fig. 2. Half-bridge LLC resonant converter operating waveforms.

t_0–t_1 stage: at the moment of $t = t_0$, the lower transistor Q_2 is turned off. At the same time, the resonant current i_{Lr} discharges the junction capacitor of the upper transistor Q_1. The body diode of Q_1 turns on, and the drain-source voltage drops to the reverse conduction voltage drop. The voltage on the excitation inductor L_m is clamped by the

voltage reflected from the secondary side, and only the resonant capacitor C_r and inductor L_r participate in the resonance.

t_1–t_2 stage: at the moment of $t = t_1$, the upper device Q_1 is conducting under zero voltage conditions. The input voltage V_{in} is added to the resonant network, and the current i_{Lr} changes sinusoidally. And the excitation current i_{Lm} increases linearly. The difference between i_{Lr} and i_{Lm} is shown in the shaded part of the figure. And the current is transmitted to the load through the high-frequency transformer after diode rectification. Since the switching period is greater than the resonant period, the resonant current i_{Lr} drops to the equivalent of the excitation current i_{Lm} before Q_1 is turned off. At the moment of $t = t_2$, the diode D_1 is turned off, and this stage ends. When the converter works with $f_s < f$, the resonance current i_{Lr} is more significant than the excitation current i_{Lm} until Q_1 is turned off.

t_2–t_3 stage: at the moment of $t = t_2$, Q_1 is still conducting, and D_1 is off. The resonant capacitor C_r, resonant inductor L_r, and excitation inductor L_m participate in the resonance. At the same time, because the resonant current i_{Lr} is equal to the excitation current i_{Lm}, the primary current of the high-frequency transformer is zero, and the primary and secondary sides are disconnected.

t_3–t_4 stage: at the moment of $t = t_3$, the upper tube Q_1 is turned off. The resonant current i_{Lr} discharges the capacitor of the lower tube Q_1 junction, and the body diode is turned on. The voltage on L_m is clamped by the voltage reflected from the secondary side, and the resonant capacitor C_r and resonant inductor L_r participate in the resonance. The resonance current i_{Lr} decreases sinusoidally, and the excitation current i_{Lm} decreases linearly.

t_4–t_5 stage: at the moment of $t = t_4$, Q_2 is turned on under zero voltage conditions. When the resonant current i_{Lr} is sinusoidal goes down to zero and then increases in the opposite direction. The excitation current i_{Lm} changes linearly from a positive maximum to a negative maximum. The resonant capacitor C_r discharges, and the stored energy is transferred to the load in the form of the difference between i_{Lr} and i_{Lm}.

t_5–t_6 stage: at the moment of $t = t_5$, i_{Lm} drops to $i_{Lr} = i_{Lm}$. At this time, diode D_2 is turned off. Because the excitation inductor L_m participates in resonance, and L_m is far greater than L_r, the resonance current remains constant until Q_2 is turned off. When Q_2 is turned off, the next cycle begins.

2.3 Fundamental Analysis and Voltage Gain

First harmonic approximation (FHA) is a method to analyze the steady-state model of the resonant converter. When the converter's switching frequency works at the resonant frequency, the resonant network shows high impedance to the higher harmonics far away from the fundamental wave of voltage and current. The energy conversion of the converter is mainly completed by the fundamental wave in the Fourier series of voltage and current. At this time, the steady-state analysis of the converter only considers the fundamental component, and the error is tiny when the converter works near f_s. The AC steady-state model of LLC Resonant Converter in fundamental analysis is shown in Fig. 4. Among them, v_{fund} is the fundamental neutral point voltage in the switching network. R_L' is the AC equivalent resistance after the load resistance, and the secondary side of the high-frequency transformer is converted to the primary side.

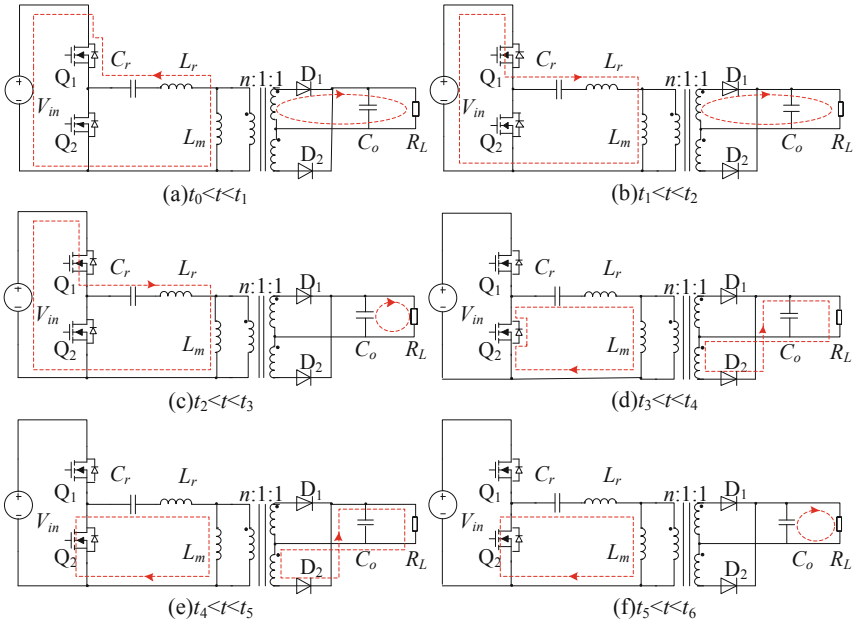

Fig. 3. Working mode analysis of half-bridge LLC resonant converter.

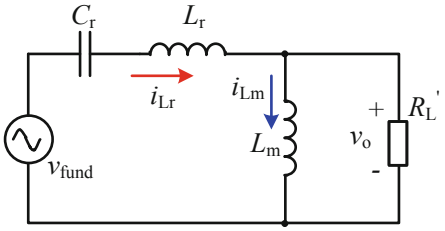

Fig. 4. AC steady-state model of a half-bridge LLC resonant converter.

The fundamental voltage is obtained by the Fourier decomposition of the neutral point voltage.

$$v_{\text{fund}} = \frac{2}{\pi} V_{\text{in}} \sin(2\pi f \cdot t) \tag{3}$$

Where, V_{in} is the DC input voltage, and f is the switching frequency of the converter. AC equivalent resistance $R_{\text{L}}{}'$ can be rewritten as follows.

$$R_{\text{L}}^{'} = \frac{8n^2}{\pi^2} \cdot R_{\text{L}} \tag{4}$$

Where, n is the transformation ratio of the high-frequency transformer and R_{L} is the value of load resistance.

According to the AC equivalent model of the half-bridge LLC resonant converter in Fig. 4, the voltage gain Mg can be obtained as follows.

$$M_{\mathrm{g}} = \left| \frac{(\mathrm{j}\omega L_{\mathrm{m}}) \| R_{\mathrm{L}}^{'}}{(\mathrm{j}\omega L_{\mathrm{m}}) \| R_{\mathrm{L}}^{'} + \mathrm{j}\omega L_{\mathrm{r}} + \frac{1}{\mathrm{j}\omega C_{\mathrm{r}}}} \right| \tag{5}$$

In order to study the influence of the parameters on the gain, the parameters are normalized.

$$M_{\mathrm{g}}(f_n, L_{\mathrm{n}}, Q_{\mathrm{e}}) = \left| \frac{L_{\mathrm{n}} \cdot f_{\mathrm{n}}^2}{\left[(L_{\mathrm{n}} + 1) \cdot f_{\mathrm{n}}^2 - 1\right] + \mathrm{j}\left[\left(f_{\mathrm{n}}^2 - 1\right) \cdot f_{\mathrm{n}} \cdot Q_{\mathrm{e}} \cdot L_{\mathrm{n}}\right]} \right| \tag{6}$$

$$f_{\mathrm{n}} = \frac{f}{f_{\mathrm{s}}}; L_{\mathrm{n}} = \frac{f_{\mathrm{m}}}{f_{\mathrm{r}}}; Q_{\mathrm{e}} = \frac{\sqrt{L_{\mathrm{m}}/L_{\mathrm{r}}}}{R_{\mathrm{L}}^{'}} \tag{7}$$

f_{n} is the normalized frequency. L_{n} is the inductance ratio. Q_{e} is the quality factor.

Figure 5 shows the relationship between the DC voltage gain M_{g} and the normalized frequency f_{n} under different loads. The difference between the switching frequency f and the load value can be divided into three different regions. When the switching frequency f is equal to the resonant frequency f_{s}, the resonant inductor L_{r} and the resonant capacitor C_{r} resonate in series. They are short-circuited, and the voltage drop is zero. The input voltage is directly applied to the excitation inductance and load, so the voltage gain is constant at 1. When the switching frequency f is less than the resonant frequency f_{s}, the resonant inductor L_{r} and the resonant capacitor C_{r} are capacitive to the outside. At this time, the larger the quality factor Q_{e} is, the heavier the load is, and the more capacitive the total input impedance is, as shown in area ① of Fig. 5. The converter can achieve ZCS on the secondary side, but the primary side will be without ZVS. The lower the quality factor Q_{e} is, the lighter the load is, and the more inductive the total input impedance

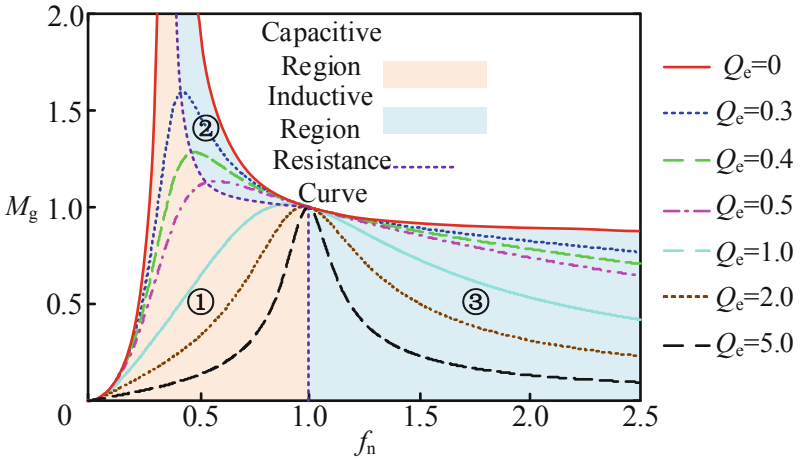

Fig. 5. Voltage gain vs. normalized frequency curves.

is. The voltage gain is greater than 1, which is shown in area ② of Fig. 5. At this time, the converter can realize ZVS on the primary side and ZCS on the secondary side. The intersection line between them is the total load curve, which is shown as a resistance. When the switching frequency f is greater than the resonant frequency f_s, the resonant inductor L_r and the resonant capacitor C_r are inductive. The excitation inductor L_m and the load capacitor parallel network are inductive, and the voltage gain is less than 1. The converter works in the inductive region, that is, region ③. The converter can achieve ZVS on the primary side but lose ZCS on the secondary side. In order to realize ZVS on the primary side, the converter should be designed to work in zone ② and zone ③.

2.4 Effect of Output Capacitance of Switch on LLC Resonant Converter

When the converter's switching frequency works at $f = f_s$ point, the resonant network voltage is zero as a whole, and the efficiency of transferring energy to the secondary side reaches the maximum value. Generally, this point is designed as the rated working state of the converter. Based on the analysis of the working condition of the converter at $f = f_s$, the dead time of the LLC resonant converter is much less than the switching cycle time. In the dead time, the primary and secondary sides are disconnected, and the excitation current i_{Lm} is equal to the resonant current i_{Lr}. The voltage on the excitation inductor is the value of the secondary side output voltage converted to the primary side, which is converted linearly in a quarter cycle and reaches the peak value in the dead time. The waveform is shown in Fig. 6, and the peak value of the primary excitation current is i_{Lm_p} can be calculated as follows.

$$I_{Lm\_P} = \frac{nV_o}{L_m} \cdot \frac{T_0}{4} \tag{8}$$

In order to realize ZVS at the primary side, the peak value of excitation current i_{Lm_p} in dead time should charge and discharge the output junction capacitance C_{oss} of Q_1 and Q_2, and the PCB distributed capacitance C_{stray} in the switching network to make the drain-source voltage drop to zero before the device is turned on.

$$I_{Lm\_P} \geq \frac{2V_{in}\left(2C_{oss} + C_{stray}\right)}{t_d} \tag{9}$$

The distributed capacitance C_{stray} of PCB is mainly the capacitance between the gate and source lying in pads and the routing line of PCB, which should be optimized in PCB plate making. Generally, its value is far less than the output junction capacitance C_{oss} of the power devices. $2C_{oss} + C_{stray} = C_{eq}$ is proposed, and Eq. (8) is substituted into Eq. (9) to get the following formula.

$$L_m \leq \frac{T_0 t_d}{16 C_{eq}} \tag{10}$$

From the above analysis, it can be seen that in $T/2$, the resonance current i_{Lr} changes according to the sinusoidal quantity, and the excitation current i_{Lm} changes linearly.

$$i_{Lr}(t) = \sqrt{2} I_{RMS\_P} \sin(\omega t + \Phi) \tag{11}$$

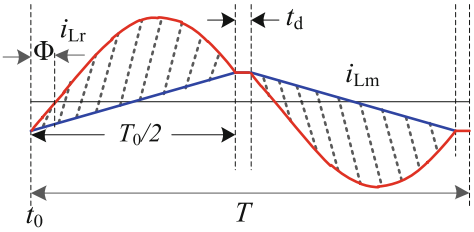

Fig. 6. Resonant current and excitation current at $f = f_s$.

Among them, I_{RMS_P} is the practical value of primary current, ω is the angular frequency of the resonant frequency, Φ is the phase difference between resonance current and excitation current. In the dead time, the excitation current i_{Lm} is equal to the resonance current i_{Lr}.

$$i_{Lr}(t_0) = \sqrt{2} I_{RMS\_P} \sin(\Phi) = -\frac{nV_0}{L_m} \cdot \frac{T}{4} \tag{12}$$

At the same time, the difference between the primary resonance current i_{Lr} and the excitation current i_{Lm} is the current transmitted to the secondary side in half a period.

$$\frac{\int_0^{\frac{T_0}{2}} \left[\sqrt{2} I_{RMS\_P} \sin(\omega_0 t + \Phi) + \frac{nV_o}{L_m}\frac{T_0}{4} - \frac{nV_o}{L_m} t\right] dt}{T/2} = \frac{V_o}{nR_L} \tag{13}$$

The excitation inductance L_m is taken as the maximum value under ZVS.

$$L_m = \frac{T_0 t_d}{16 C_{eq}} \tag{14}$$

From Eq. (13) and Eq. (14), the relationship among the practical values of primary current I_{RMS_P}, C_{eq}, and dead time t_d can be obtained.

$$I_{RMS\_P} = \frac{1}{4\sqrt{2}} \frac{V_o}{nR_L} \sqrt{\frac{256 C_{eq}^2 n^4 R_L^2}{t_d^2} + 4\pi^2 + \frac{16\pi^2 (T_0 t_d + t_d^2)}{T_0^2}} \tag{15}$$

The RMS of the secondary side current is the current transferred to the secondary side by the difference between the resonance current i_{Lr} and the excitation current i_{Lm}.

$$\begin{aligned} I_{RMS\_S} &= \sqrt{\frac{\int_0^{\frac{T_0}{2}} [i_{Lr}(t) - i_{Lm}(t)]^2 dt}{T_S/2}} \\ &= \frac{\sqrt{3}}{24\pi} \frac{V_O}{R_L} \sqrt{\frac{256 C_{eq}^2 (5\pi^2 - 48) n^4 R_L^2 T_0}{t_d^2 (T_0 + 2t_d)} + \frac{12\pi^4 T_0}{T_0 + 2t_d} + \frac{48\pi^4 (T_0 t_d + t_d^2)}{T_0 (T_0 + 2t_d)}} \end{aligned} \tag{16}$$

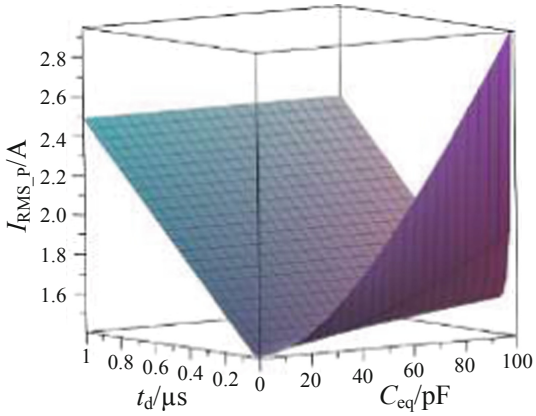

Fig. 7. Relationship between the RMS current of the primary side and C_{eq} and t_d.

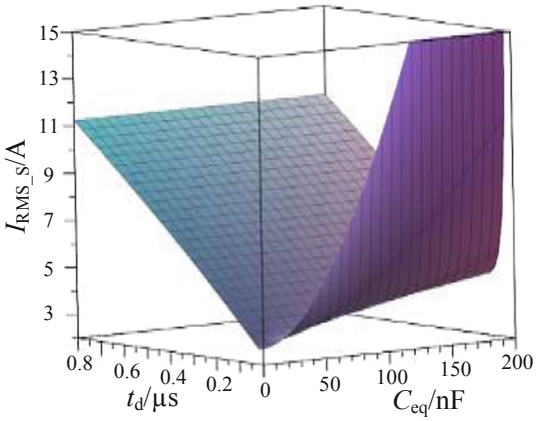

Fig. 8. Relationship between the RMS current of the secondary side and C_{eq} and t_d.

The current RMS determines the conduction loss of the primary side and secondary side switching devices and rectifier diodes. In the case of ZVS on the primary side and ZCS on the secondary side, the conduction loss accounts for an essential part of the total loss of the converter. Reducing the RMS current of the primary and secondary side is of great significance to improve the converter's efficiency. Figure 7 and Fig. 8 respectively draw the graphs of the primary and secondary side current practical value changing with the equivalent capacitance C_{eq} and dead time t_d by Maple mathematical software. It can be seen that under the condition of a specific dead time t_d, the primary and secondary side currents have a minimum value. And with the increase of C_{eq}, the primary and secondary side current also increases. Since C_{eq} is mainly composed of the output capacitance C_{oss} of switching devices, the smaller output capacitance of C_{oss} corresponds to the smaller RMS currents of the primary and secondary sides. It is of great significance to reduce the conduction loss and transformer loss of the converter and

improve its efficiency. Compared with Si MOSFET, the cascade GaN HEMT has smaller output capacitance C_{oss}, so it has positive significance for LLC resonant converter to reduce loss and improve efficiency.

According to the output capacitance of the cascode GaN HEMT TPH3206PSB and Si MOSFET IPI60R199CP, the change of RMS current at primary and secondary sides of LLC resonant converter with dead time is obtained, as shown in Fig. 9. It can be seen that the optimal dead time of Si MOSFET is about 200ns, and the optimal dead time of GaN device is about 100ns. Compared with Si MOSFET, the RMS of the primary current for GaN device is less than 0.2A, and the RMS of the secondary current is less than 1.5A. It can be seen that the design of LLC resonant converter using GaN device results in the turn-off loss reduction of the converter due to the excellent switching characteristics of the devices. The circulating current of the converter is effectively reduced. The loss of the converter decreases, and the efficiency of the converter due to its small output capacitance is improved (Fig. 10).

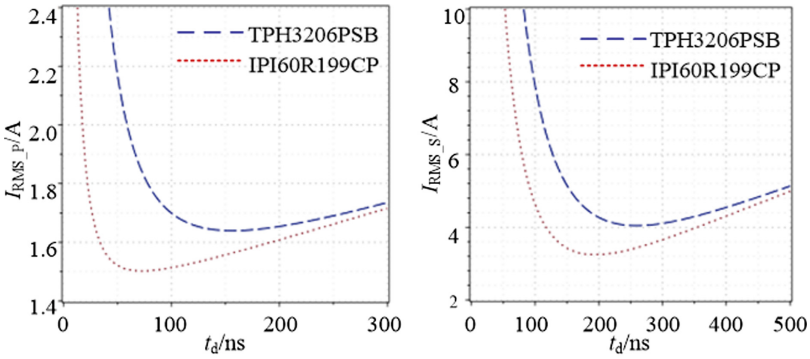

Fig. 9. Relationship between RMS current and dead time for different output capacitors.

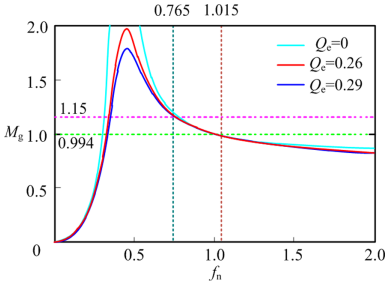

Fig. 10. Parameter design verification.

3 Experimental Verification and Loss Analysis

3.1 Experimental Verification

A half-bridge LLC resonant converter based on the cascode GaN HEMT TPH3206PSB is built. It is tested under different load conditions, and the working waveforms of the converter are shown in Fig. 11. The energy increases with the growth of the load, which is transferred from the converter to the load. The resonant current rises, and the primary side cycle energy increases. The converter can realize ZVS at the primary side in the full load range. Compared with hard-switching applications, the peak and oscillation problems in soft switching applications vanish, and the stability of the converter is greatly improved. At the same time, the efficiency of the converter under different loads is tested. As shown in Fig. 12, the maximum efficiency of the converter can reach 97%, and the full load efficiency of 96.2% is achieved.

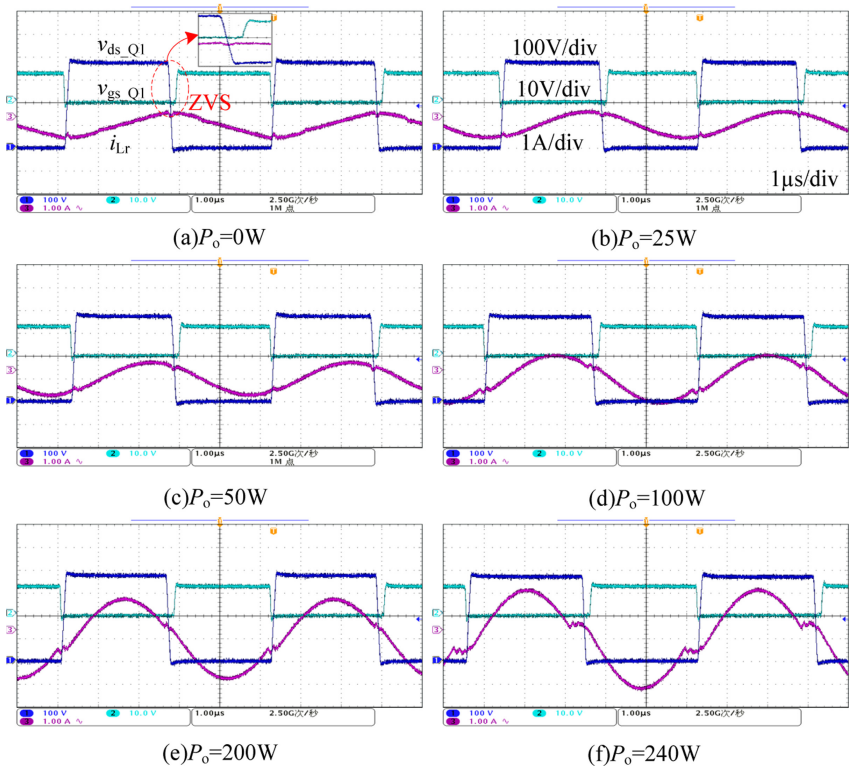

Fig. 11. Converter operating waveforms under different loads.

3.2 Loss Analysis

In order to make further efforts on the influence of the cascode GaN HEMT on LLC resonant conversion, the loss of the converter is analyzed.

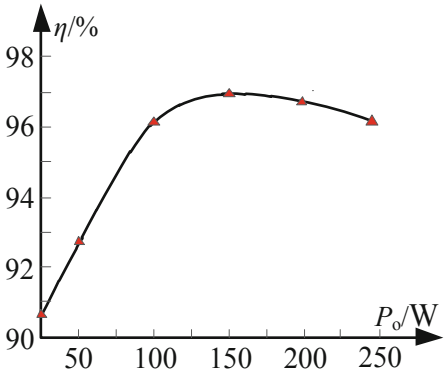

Fig. 12. Converter efficiency curve.

(1) Switching losses. It mainly includes device switching losses P_{switch}, conduction losses P_{con}, and driving losses P_{dri}.

Since ZVS is realized on the primary side of the converter, the switching loss only includes the turn-off loss. It can be seen from the previous paper that the turn-off loss is very small and can be ignored.

$$P_{\text{con\_Q}} = I_{\text{RMS\_P}}^2 \cdot R_{\text{ds\_Q}} \tag{17}$$

$$P_{\text{dri\_Q}} = V_{\text{D}} \cdot Q_{\text{g}} \cdot f_{\text{s}} \tag{18}$$

Among them, the primary side current $I_{\text{RMS\_P}}$ is given by Eq. (11). $R_{\text{ds\_Q}}$ is the conducting resistance. V_{D} is the driving voltage, and Q_{g} is the gate driving charge.

(2) Loss of synchronous rectifier. The synchronous rectification is adopted on the secondary side of the converter. Since ZCS is realized on the secondary side, the body diode of the synchronous rectifier has been conducting before the rectifier operates, which is equivalent to ZVS. The switching loss of the synchronous rectifier can be ignored, so the loss of the synchronous rectifier is mainly the conduction loss $P_{\text{con\_SR}}$, drive loss $P_{\text{dri\_SR}}$.

$$P_{\text{con\_SR}} = I_{\text{RMS\_S}}^2 \cdot R_{\text{ds\_SR}} \tag{19}$$

$$P_{\text{dri\_SR}} = V_{\text{D}} \cdot Q_{\text{g}} \cdot f_{\text{s}} \tag{20}$$

Where, $R_{\text{ds\_SR}}$ is the conducting resistance of the synchronous rectifier, and the calculation of the driving loss $P_{\text{dri\_SR}}$ is consistent with the primary side.

(3) Loss of magnetic devices. In this paper, the excitation inductance and resonant inductance are designed as leakage inductance and excitation inductance of the high-frequency transformer. The loss of magnetic devices is mainly copper loss P_{Cu} and iron loss P_{Fe} of the high-frequency transformer. The copper loss P_{Cu} is obtained as follows.

$$P_{\text{Cu}} = R_{\text{Cu\_P}} \cdot I_{\text{RMS\_P}}^2 + R_{\text{Cu\_S}} \cdot I_{\text{RMS\_S}}^2$$

$$= 2\sigma j N_P \sqrt{\pi A_e} I_{RMS\_P} + 2\sigma j N_S \sqrt{\pi A_e} I_{RMS\_S} \tag{21}$$

Among them, σ is the copper resistivity. N_P and N_S are the primary and secondary turns, respectively. j is the current density. A_e is the conductor cross-sectional area. The iron loss P_{Fe} is calculated in Eq. (22).

$$P_{Fe} = P_v \cdot V_e = k \cdot f^m \cdot B_p^n \cdot V_e \tag{22}$$

Where, P_v is the magnetism core specific loss. k, m, and n are constants. f is the equivalent frequency. B_p is the flux density. V_e is the effective volume of the core. The loss of each part of the converter is calculated as shown in Fig. 13.

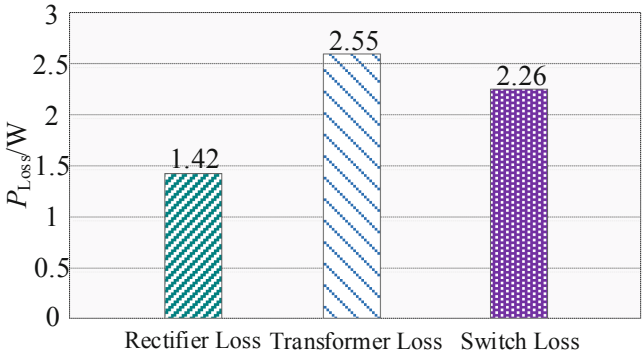

Fig. 13. LLC resonant converter loss analysis.

In LLC resonant converter based on the cascode GaN HEMT, the device loss does not account for most of the converter loss, and the high-frequency transformer loss becomes the most significant part of the system loss under full load. Therefore, to further improve the converter's efficiency, it is necessary to use a planar high-frequency transformer to reduce the transformer loss further.

4 Conclusions

The ccascode GaN HEMTs are applied to LLC resonant converter with the soft-switching topology. The relationship between dead time, primary and secondary current RMS, and output capacitance is analyzed. At the same time, relying on the advantage of cascode GaN HEMT with small output capacitance, the soft-switching condition of the LLC resonant converter is improved. The RMS current of the primary and secondary sides is reduced. The conduction loss and transformer loss are further reduced. The converter efficiency is improved. The hardware platform of 240W LLC resonant converter based on the cascode GaN HEMT is built. The maximum efficiency of the converter is 97%, and the total load efficiency can reach 96.2%. The loss of each part of the converter is analyzed, and the direction of further improving the efficiency of the converter is proposed.

Acknowledgements. The authors acknowledge the Jiangsu University Natural Science Research Project (18KJB470024) and Provincial Construction System Science and Technology Project of Jiangsu Provincial Housing and Urban-Rural Construction Department (2018ZD088). This work is partly supported by the Natural Science Foundation of Jiangsu Province of China (No. BK20161165), the applied fundamental research Foundation of Xuzhou of China (No. KC17072). The authorized patents for invention are also the research and development of Jiangsu Province Industry-University-Research Cooperation Project (BY2019056).

References

1. Huang, X., Liu, Z., Qiang, L., Lee, F.C.: Evaluation and application of 600V GaN HEMT in cascode structure. In: 2013 Twenty-Eighth Annual IEEE Applied Power Electronics Conference and Exposition (APEC). IEEE (2013)
2. Huang, X., Liu, Z., Qiang, L., Lee, F.C.: Evaluation and application of 600V GaN HEMT in cascode structure. APEC 2013 (2013)
3. Zhang, W., Xu, Z., Zhang, Z., Wang, F., Blalock, B.J.: Evaluation of 600 V cascode GaN HEMT in device characterization and all-GaN-based LLC resonant converter. In: Energy Conversion Congress and Exposition. IEEE (2013)
4. Sugiyama, T., Hung, H., Isobe, Y., Yoshioka, A., Ikeda, K.: Stable cascode GaN HEMT operation by direct gate drive. In: 2020 32nd International Symposium on Power Semiconductor Devices and ICs (ISPSD). IEEE (2020)
5. Zhang, W., Wang, F., Tolbert, L.M., Blalock, B.J., Costinett, D.: Investigation of soft-switching behavior of 600 V cascode GaN HEMT. In: 2014 IEEE Energy Conversion Congress and Exposition (ECCE). IEEE (2014)
6. Li, Q., Liu, B., Duan, S.: Simplified analytical model for estimation of switching loss of cascode gan hemts in totem-pole pfc converters. Chin. J. Electr. Eng. **5**(3), 1–9 (2019)
7. Liu, Z.: Characterization and failure mode analysis of cascode gan HEMT. Virginia Tech (2014)
8. Katzir, L., Shmilovitz, D.: A 1-MHZ 5-kV power supply applying SiC diodes and GaN HEMT cascode mosfets in soft switching. IEEE J. Emerg. Sel. Top. Power Electron. **4**(4), 1474–1482 (2016)
9. Huang, X., Li, Q., Liu, Z., Lee, F.C.: Analytical loss model of high voltage gan hemt in cascode configuration. IEEE Trans. Power Electron. **29**(5), 2208–2219 (2014)
10. Wang, N., Jia, H., Tian, M., Li, Z.W., Xu, Y.: Impact of transformer stray capacitance on the conduction loss in a GaN-based LLC resonant converter. In: 2017 IEEE 3rd International Future Energy Electronics Conference and ECCE Asia (IFEEC 2017 - ECCE Asia). IEEE (2017)
11. Liu, Z., Huang, X., Lee, F.C., Qiang, L.: Simulation model development and verification for high voltage GaN HEMT in cascode structure. In: Energy Conversion Congress and Exposition. IEEE (2013)
12. Park, H.P., Jung, J.H.: Design considerations of 1 MHz LLC resonant converter with GaN E-HEMT. In: European Conference on Power Electronics & Applications. IEEE (2015)
13. Xiang, J., Ren, X., Wang, Y., Yue, Z.: Investigation of cascode stucture GaN devices in ZCS region of LLC resonant converter. In: 2017 IEEE Energy Conversion Congress and Exposition (ECCE). IEEE (2017)
14. Cheng, S., Chou, P.C.: Power conditioning applications of 700V GaN-HEMTs cascode switch. In: Conference of the IEEE Industrial Electronics Society. IEEE (2016)

15. Huang, X., Qiang, L., Liu, Z., Lee, F.C.: Analytical loss model of high voltage GaN HEMT in cascode configuration. In: 2013 IEEE Energy Conversion Congress and Exposition. IEEE (2013)
16. Attia, Y., Youssef, M.: GaN on silicon E-HEMT and pure silicon MOSFET in high frequency switching of EV DC/DC converter: a comparative study in a nissan leaf. In: 2016 IEEE International Telecommunications Energy Conference (INTELEC). IEEE (2016)
17. Li, Q., Liu, B., Duan, S., Wang, L., Luo, C.: Analytical switching loss model of cascode GaN HEMTs based totem-pole PFC converters considering stray inductances. In: 2018 1st Workshop on Wide Bandgap Power Devices and Applications in Asia (WiPDA Asia). School of Electrical and Electronic Engineering, Huazhong University of Science and Technology, Wuhan (2018)
18. Galanos, N., Popovic, J., Ferreira, J.A., Gerber, M.: Influence of the magnetic's parasitic capacitance in the switching of high-voltage cascode GaN HEMT. In: Cips, International Conference on Integrated Power Electronics Systems. VDE (2016)
19. Chou, P.-C., Cheng, S.: Performance characterization of gallium nitride hemt cascode switch for power conditioning applications. Mater. Sci. Eng. B (2015)